European Journal of Pharmaceutics and Biopharmaceutics 140 (2019) 78–90

Contents lists available at ScienceDirect

European Journal of Pharmaceutics and Biopharmaceutics

journal homepage: www.elsevier.com/locate/ejpb

Research paper

# Cocrystals of curcumin-isonicotinamide and curcumin-gallic acid: Does the weak forces in cocrystals effect on binding profiles with BSA and cell cytotoxicity?

Wenzhe Pang[a,b], Yarong Wu[a], Na Xue[a], Ying Li[c], Shuang Du[a], Binnan He[a], Caiqin Yang[a], Jing Wang[a,*], Yanli Zeng[c,*]

[a] School of Pharmaceutical Sciences, Hebei Medical University, Shijiazhuang 050017, People's Republic of China
[b] Hebei Institute of Drug Control and Research, Shijiazhuang 050011, People's Republic of China
[c] College of Chemistry and Material Science, Hebei Normal University, Shijiazhuang 050024, People's Republic of China



ARTICLE INFO

*Keywords:*
Cocrystals
Curcumin
Bioavailability
Cell cytotoxicity
Bovine serum albumin

ABSTRACT

Screening of cocrystal has been proved to be a powerful approach to improve the solubility, dissolution rate and even the bioavailability of poorly water-soluble active pharmaceutical ingredient (API). Typically, the formation of cocrystal induces no change on the pharmacological profile of the APIs. However, so far, it is not clear whether a cocrystal would induce changes in biological profiles of API and, if so, which factors induce those changes. To clarify these aspects, two CUR-isonicotinamide (cocrystal 1) and CUR-gallic acid (cocrystal 2) cocrystals with enhanced physical properties and pharmacokinetic profile for potential pharmaceutical application were screened. We focused on the effects of the type of hydrogen bonds occurred in cocrystal on the binding between cocrystal and BSA as well as cell inhibiting activity. The appearance of new peaks in the X-ray powder diffraction (PXRD) and a single different melting point in the differential scanning calorimetry (DSC) measurements revealed that homogeneous, single phase formulations were obtained by forming cocrystals between CUR and coformers in a 1:2 M ratio. The results of Fourier-transform infrared and solid-state $^{13}C$ nuclear magnetic resonance spectra as well as density function theory simulation indicated that different hydrogen bonds were formed in two cocrystal, which were the C═O···H−N hydrogen bond between the C═O group in CUR and the N−H groups in isonicotinamide in cocrystal 1, and C═O···H−O hydrogen bond between phenol O−H group in CUR and the C═O group in gallic acid in cocrystal 2, respectively. Interestingly, the different type of weak interactions in cocrystal induced various binding pattern between cocrystal and BSA and cancer cell cytotoxicity supported by fluorescence spectroscopy and MTT assay in vitro. It was reasonable that the affinity of cocrystal for proteins varied with specific and concerted weak interactions in cocrystal, which would induce changes in the biological profiles of the parent drug. Furthermore, in vivo pharmacokinetics of CUR and CUR-based cocrystals in SD rats were evaluated through UPLC-MS/MS method. Compared with intact CUR, the pharmacokinetics parameters $C_{max}$, $T_{max}$, $AUC_{0-t}$ and $AUC_{0-\infty}$ of CUR-based cocrystals were improved ($P < 0.05$); $C_{max}$ increased 30-fold, $T_{max}$ shortened 6-fold, and $AUC_{0-t}$ increased 6-fold. Overall, the present results inferred different effects induced by cocrystals on a biologic system, not only bioavailability but biological profiles.

## 1. Introduction

Curcumin (CUR) is a kind of plant polyphenols which is extracted from the rhizome of turmeric [1]. It exhibits diverse pharmacological activities, such as anticancer, hypoglycemic effect, antiulcer, anti-inflammatory and antibacterial [2,3]. The main advantage of CUR is being safe at high dose of 12 $g \cdot day^{-1}$ in humans. Nevertheless, the therapeutic effectiveness of CUR is limited by the very low solubility and poor bioavailability in the aqueous medium. Pharmaceutical cocrystals are supramolecular complexes which are formed from active pharmaceutical ingredient (API) and the small molecule cocrystal formers (CCF) through non-covalent interactions involving hydrogen bonds and van der waals forces [4,5]. Pharmaceutical cocrystals keep the intact structure and pharmacological activities of API, while, create

* Corresponding authors.
*E-mail addresses:* jingwang@home.ipe.ac.cn (J. Wang), yanlizeng@hebtu.edu.cn (Y. Zeng).

https://doi.org/10.1016/j.ejpb.2019.05.005
Received 11 January 2019; Received in revised form 3 April 2019; Accepted 8 May 2019
Available online 11 May 2019
0939-6411

advantages on solubility, dissolution rates and even bioavailability and tableting characteristics [6–8]. Supramolecular complexes are promising solid form and have attracted considerable attention for improving the physicochemical properties of APIs.

CUR has been reported to form cocrystals with several coformers such as nicotinamide, isonicotinamide, piperazine, hydroquinone, 4, 4′-bipyridine-N, N′-dioxide, resorcinol, pyrogallol, etc. [9–12]. For example, the intrinsic dissolution rate (IDR) of CUR-pyrogallol cocrystal was 0.094 $(mg/cm^2)\cdot min^{-1}$, which increased 12-fold than that of intact CUR. It was also reported that a drug-drug coamorphous phase, namely CUR-artemisinin coamorphous, exhibited a 2.6 times IDR than that of intact CUR, and the pharmacokinetic characteristics of CUR were significantly improved ($AUC_{0\text{-}12}$: 2.6 μg·h·mL$^{-1}$, $C_{max}$: 1 μg·mL$^{-1}$) [13]. Besides, CUR-folic acid coamorphous complex showed higher solubility than that of parent crystalline pure CUR [14].

In our previous study, the formation of CUR-piperazine coamorphous phase with improved dissolution rates was reported [15]. Piperazine was chosen as co-former because it is commonly used pharmaceutical intermediates and has piperazine ring with imino group (hydrogen donor). Unfortunately, the introduction of piperazine into the coamorphous phase dramatically lowered the $T_g$ of amorphous CUR. Although the CUR-piperazine coamorphous shows higher dissolution rate than that of single CUR, the lower $T_g$ limits pharmaceutical application. Moreover, the investigation on interaction between CUR-piperazine coamorphous and BSA indicated that the binding affinity between CUR and BSA changed with introduction of piperazine. These results present important hint that the weak interaction between API and coformer would induce changes in the biological profiles of the APIs.

Particularly, it is not yet clear whether a cocrystal would be defined as a new chemical entity requiring full safety and toxicology assay or just their parent physical mixture [16,17]. Fortunately, researcher are realizing the problem and giving concerns about performing appropriate investigations before using of cocrystal to improve API bioavailability. A. Dalpiaz et al. performed a systematic comparison among indomethacin, its cocrystals, and their parent physical mixtures on dissolution profile, the ability to permeate across intestinal cell monolayers (NCM460), and oral bioavailability [18]. It was clearly evidenced that the biological effects of a cocrystal and its parent mixture were different, such as the TEER value of NCM460 cell monolayers, although definite reason(s) for these phenomena was not presented and general rule of difference on cocrystal entity and simple physical mixture was not obtained.

In present study, we aim to screen more stable CUR-based cocrystal supramolecules to improve the physiochemical properties of CUR. The CUR- isonicotinamide (cocrystal 1) and CUR-gallic acid (cocrystal 2) cocrystals were successfully screened using ethanol-assisted grinding. Since CUR-isonicotinamide cocrystal was reported in the patent WO 2015/052568A2 [10], in which reflux method in ethyl acetate was used, different preparing method is expected to produce novel structure. The schematic representations of CUR and CCFs are presented in Fig. 1. The main objective was to find out if the weak interactions (here commonly hydrogen bonds) between CUR and CCF induce the changes on the biological profiles of the CUR. Here, we focus on the relationships of the type of hydrogen bonds occurred in cocrystal and the binding between CUR-CCF cocrystal and BSA as well as cell inhibiting activity.

It has been reported that oral CUR stays in the colon for a longer time, more studies on CUR focus on colon cancer [19]. Furthermore, the extensive cytotoxic effect of CUR is one of the main aspects of its antitumor effect [20,21]. In vitro cytotoxic experiments on various cell lines have found that CUR inhibits tumor cells at concentrations ranging from micromolar level to millimolar level [22,23]. In this study, besides human colon cancer cells (HT-29), lung cancer cells (A549) and hepatoma cells (Hepg) were used to compare the inhibitory effects of CUR and its cocrystals, as a result, to detect the relationship of weak interaction in cocrystal and the cell cytotoxic effect for different kinds cells.

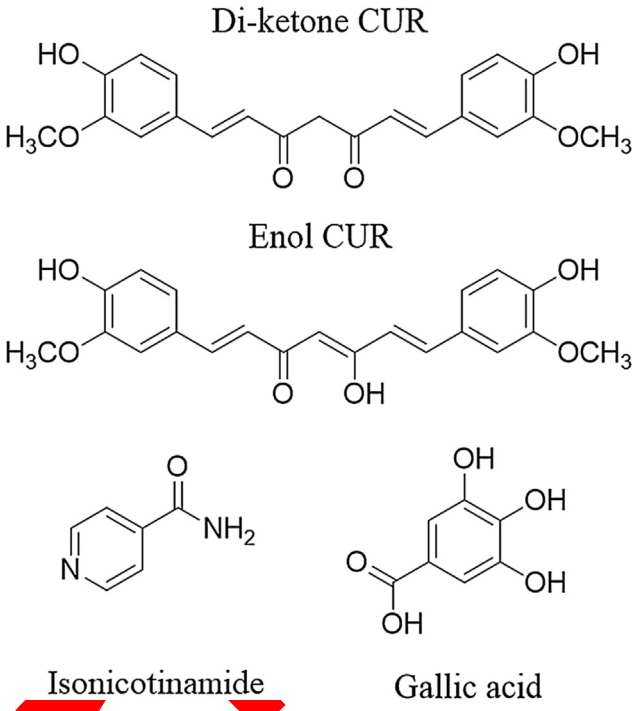


**Fig. 1.** Chemical structures of CUR isomers and CCFs.

## 2. Materials and methods

### 2.1. Materials

CUR (purity ≥ 65%) was purchased from Sigma (ALDRICH, Shanghai). Isonicotinamide was supplied by Jingchun Chemical Reagents Factory (Shanghai, China). Gallic acid was supplied by J&K Chemicals Ltd (Beijing, China). β-estradiol and fatty-acid-free bovine serum albumin (BSA, 99% purity) lyophilized powder were both acquired from Sigma Co. Ltd. (ALDRICH, Shanghai). HT-29 cell was purchased from ATCC cell library. A549 cells and Hepg cells were kindly provided by Hebei medical university, China. Methyl thiazolyl tetrazolium (MTT) was provided by Shanghai Golden Bank Biological Technology Co. Ltd. (Shanghai, China).

### 2.2. Experimental animals

Male specific pathogen-free Sprague-Dawley (SD) rats weighing 250 ± 10 g were obtained from Shanghai Slake Laboratory Animal Co. Ltd. Animals were kept in an environmentally controlled breeding room (temperature: 295–297 K, relative humidity: 50 ± 5%). Diet was prohibited for 12 h before the experiment, while water was taken freely. All animal tests follow the guiding principles of the experimental animal management committee of Hebei Medical University.

### 2.3. Methods

#### 2.3.1. Preparation of cocrystal 1 and 2

The cocrystal samples were prepared by EtOH-assisted oscillatory ball milling method using a laboratory-scale oscillatory ball mill (Mixer Mill GT200, Grindertech GmbH, Beijing, China) as described in Ref [15]. Briefly, total weighted 500 mg of CUR/CCFs (isonicotinamide or gallic acid) mixtures, with the molar ratios of 2:1, 1:1, and 1:2, respectively. The sample was ground in a 35 mL zirconia grinding jar with 1.5 cm of zirconia grinding ball at a speed of 1800 rpm. During the

grinding procedure, ethanol was added to the grinding jar to keep the mixture powder the slurry state. The product was collected after 30 min grinding and then dried at 313 K in vacuum oven for 4–5 h.

*2.3.2. X-ray powder diffraction (PXRD)*

PXRD was performed on Bruker D2 Advance diffractometer (D2 Phaser, Bruker Co., Germany) using Cu Kα radiation (λ = 1.54187 Å) and Lynx eye detector. The patterns were collected from 5 to 40° (2*θ*) with a step size of 0.05° (2*θ*) and time per step of 0.3 s.

*2.3.3. Scanning electron microscopy (SEM)*

Cryo-field emission SEM was recorded on cryo-emission SEM system (Hitachi S-4800, Japan). Single CUR powder or cocrystal was dissolved in ethanol to form a suspension. Then, by dropping the resulting suspension onto the electric glass slice, the micromorphologies of single CUR and its cocrystals were observed by SEM after the solvent volatilized.

*2.3.4. Thermal analysis*

Differential scanning calorimetry (DSC) was recorded on DSC 214 (NETZSCH Company, Germany) equipped with IC40 refrigerated cooling accessory and Proteus Analysis 7.0 data analyzer under the nitrogen atmosphere at a flow rate of 20 mL·min$^{-1}$. Total weight of about 6 mg of CUR or cocrystal was sealed in an aluminum pan, which was subjected to thermal scanning at a heating rate of 20 K·min$^{-1}$ in the temperature interval of 298–573 K. Thermogravimetric (TG) experiment was performed on a TG 209 gravimetric analysis instrument (NETZSCH company, Germany) with a heating rate of 10 K·min$^{-1}$, scanning from 298 to 523 K under nitrogen purge at a flow rate of 20 mL min$^{-1}$.

*2.3.5. Fourier-transform infrared spectroscopy (FTIR)*

FTIR spectra was performed on a Prestige-21 FT-IR spectrometer (Shimadzu Co. Japan). The sample was scanned from 4000 to 400 cm$^{-1}$ at an interval of 2 cm$^{-1}$. The total number of scans was 40 and the resolution was 2 cm$^{-1}$.

*2.3.6. $^{13}C$ solid-state NMR spectroscopy (ssNMR) and $^{1}H$ time domain NMR(TD NMR)*

$^{13}$C ssNMR characterizations of CUR, cocrystals 1 and 2, as well as their respective CCF, isonicotinamide and gallic acid, were conducted on a Bruker AVANCE III NMR spectrometer (Bruker, Germany) using cross polarization pulse sequence/high power decoupling/magic angle spinning (CP/MAS) probe at 400 MHz. An adequate signal-to-noise ratio was obtained by multiple scans. The external secondary standard referenced to the methylene carbon of glycine, and then recalibrated the chemical shifts to the TMS scale ($\delta_{glycine}$ = 43.3 ppm). All ssNMR experiments were performed at room temperature.

All proton TD NMR experiments were conducted on a Bruker minispec mq20 with $^{1}$H larmor frequence of 19.95 MHz. The 90° and 180° pulse lengths were set as 2.78 and 5.2 μs, respectively. The recycle delay was set as 15 s, and the number of scan was set as 64. The inversion recovery pulse sequence was used to obtain the spin-lattice relaxation time $T_1$ of different samples. The measurement temperatures were maintained as 25.0 ± 0.5 °C.

*2.3.7. Apparent solubility determination*

The apparent solubility experiments of single CUR and its cocrystals in 0.1 mol·L$^{-1}$ HCl and 30% EtOH-$H_2O$ solution were performed by shake-flask method on SPH-200B air bath shaker (Shiping Tech. Co., Ltd., Shanghai, China) in 310 ± 0.5 K air bath. Firstly, by plotting absorbance vs concentration for known concentration solutions in 0.1 mol·L$^{-1}$ HCl and 30% EtOH-$H_2O$ solution, the calibration curves were obtained for CUR and two cocrystals using a UV-2450 UV–vis spectrometer (Shimadzu Co. Japan). The UV–vis spectra from 200 to 500 nm showed that maximum absorption wavelengths of single CUR, isonicotinamide, gallic acid and cocrystals were at 430, 268, 265 and 430 nm, respectively (Figure was not shown). The maximum absorption wavelengths of CUR dissolved from cocrystal displayed no obvious shift comparing with that of single CUR, indicating the isonicotinamide and gallic acid did not interfere with the determination of CUR, although there may be interaction weak forces between CUR and CCF in solution. An excess amount of the sample was added to 10 mL of 0.1 mol·L$^{-1}$ HCl and 30% EtOH-$H_2O$ solution, respectively. After 24 h shaking, the suspension was filtered via 0.22 μm microfiltration membrane. The filtered aliquots were diluted sufficiently, and then measured the absorbance at the given $\lambda_{max}$ of 430 nm. Each test was repeated thrice.

*2.3.8. Powder dissolution rate determination*

The powder dissolution rate determination for the CUR and its cocrystals were performed on ELECTROLAB dissolution tester system (Electrolab Technology, Co., Ltd., India) using paddle method in 0.1 mol·L$^{-1}$ HCl and 30% EtOH-$H_2O$ solution, respectively. Approximately 30 mg of the compound (here single CUR or its cocrystal equivalent to 30 mg of pure CUR) was taken in the dissolution tester that contained 900 mL of dissolution media at 310 ± 0.5 K. The paddle rotation speed was fixed at 100 rpm. At settled intervals, 5 mL of dissolution medium was withdrawn followed replacement with the same volume fresh medium. The collected receptor medium was filtered via 0.22 μm microfiltration membrane, and then determined the concentrations of CUR at 430 nm utilizing UV–vis spectrophotometer. All test was repeated thrice.

*2.3.9. Simulated calculation on optimization molecular interactions*

Simulated calculations were performed on cocrystal 1 and 2 to obtain the structure of the complex. The initial structures of CUR, isonicotinamide, and gallic acid were created from the crystal structure and then optimized at the DFT(B3LYP) theoretical level combined with the 6-31G(d,p) basis set using the GAUSSIAN-03 program package [24]. The geometries of the cocrystal 1 and 2 were constructed and optimized at same computational level.

*2.4. Fluorescence spectroscopic studies on the interaction of the cocrystals with bovine serum albumin (BSA)*

BSA stock solution was prepared by Tris-HCl buffer solution (mixing 0.10 mol·L$^{-1}$ HCl and 0.10 mol·L$^{-1}$ Tris base, then adjusting the pH value to 7.4). The final BSA stock solution with the concentration of $5 \times 10^{-5}$ mol·L$^{-1}$ was kept in the dark at 4 °C. The stock solutions of CUR and cocrystals with finally CUR equivalent concentration of $1 \times 10^{-3}$ mol·L$^{-1}$ were prepared by dissolving the CUR or cocrystal in ethanol. 1.0 mL $5 \times 10^{-5}$ mol·L$^{-1}$ BSA solution and various volumes of CUR (or cocrystal) was added to the volumetric flask and the concentrations of CUR were ranged from $2 \times 10^{-6}$ to $4 \times 10^{-5}$ mol·L$^{-1}$ by diluting with Tris-HCl buffer solution to volume. Then, the volumetric flask was shaken for 30 min at 298, 310, and 315 K air bath, respectively. Fluorescence emission spectra were measured on a F-7000 spectrofluorophotometer (HITACHI, Japan) equipped with 1.0 cm quartz cells. All fluorescent emission spectra were measured from 220 to 450 nm upon excitation at 280 nm with slit width of 3 nm at 298, 310, and 315 K, respectively. Besides, the synchronous fluorescent spectra of BSA based on various concentrations of CUR was scanned at Δλ = 15 nm and Δλ = 60 nm, respectively, with the emission and excitation slit widths of 5/5 mm.

*2.5. UPLC-MS/MS analysis*

The UPLC-MS/MS analysis was performed on liquid chromatographic system (Thermo, USA) with photodiode assay (PDA) detector together with an automatic liquid chromatographic sampler and an auto injection system hyphenated to a PRBITRAP ELITE triple quadrupole mass spectrometer (Thermo, USA) equipped with an

electrospray ionization (ESI) source. The analytical column $C_{18}$ (Hypersill, 100 mm × 2.1 mm, 1.9 μm) was used. The gradient elution conditions are listed in *Table S1 (Supporting Information)*. The volume of injection was 10 μL, with flow rate of 0.3 mL·min$^{-1}$.

For the operation in MS/MS mode, a mass spectrometer with an orthogonal Z-spray ESI was used. The analyte infusion experiment was performed using a Mode 22 multiple syringe pump (Harvard, Holliston, MA, USA). During the analysis, the ESI parameters were set as follows: source temperature: 623 K, capillary voltage: 2.75 kV for negative mode, Sheath velocity: 35 L·min$^{-1}$, auxiliary gas velocity: 10 L·min$^{-1}$, nebuliser pressure: 6.0 Bar, desolvation gas flow: 700 L·hr$^{-1}$. The interface heated and multi-reaction monitoring mode (MRM) was adopted.

### 2.6. Pharmacokinetics in vivo

A set of 18 male SD rats were randomly divided into three groups, namely, CUR group, cocrystal 1 group and cocrystal 2 group, respectively. Each rat was given CUR or cocrystals with the amount of 200 mg·kg$^{-1}$ by intragastric administration at a dose of 5 mL·kg$^{-1}$. 100 μL of blood sample from the retrobulbar venous plexus was collected into heparinized tubes at time intervals of 5, 15, 30, 45 min, 1, 2, 4, 6, 8, 12, 24 h and immediately separated by centrifugation at 5000 rpm for 10 min. All processed samples were stored at 193 K for further analysis. Calibration standards were obtained in concentration of 0.3, 1, 3, 10, 30, 100 and 300 ng·mL$^{-1}$ of CUR. The mean pharmacokinetic parameters were calculated by WinNonlin software.

### 2.7. MTT assay

The inhibitory effects of CUR and its cocrystals on human colon cancer cells (HT-29), lung cancer cells (A549) and hepatoma cells (Hepg) were evaluated by MTT assay. The cells were cultured in Dulbecco's MEM medium supplemented with 10% heat inactivated Newborn calf serum (including streptomycin 100 U·mL$^{-1}$ and penicillin 100 U·mL$^{-1}$) in a humidified 5% incubator at 310 K.

HT-29, A549 and Hepg cells were seeded into flat-bottomed adherent 96-well cell culture plates (5 × $10^4$ cells, respectively) and incubated overnight. Then, the cells were treated with various concentrations of CUR (5, 10, 20, 30, 40, 50, 60 μM) for 24 h. Subsequently, the culture medium was abandoned and medium was carefully replaced by 0.5% 3-[4,5-dimethylthiazol-2-yl]-2,5-diphenyltetrazoliu bromide (MTT) added in each hole, then incubated for 3 h. Formazan crystals resulting from MTT reduction were dissolved by adding 100 μL DMSO and gently agitating for 10 min. The absorbance (OD) was measured at a wavelength of 595 nm with a reference wavelength of 630 nm. Cell viability was calculated as the percentage of the control, that is, the untreated cells. Each test was repeated at least three times.



### 2.8. Statistical analysis

The SPSS 21.0 software was used to carry out statistical analysis and variance analysis. Results with $P < 0.05$ showed that the difference was statistically significant.

## 3. Results and discussion

### 3.1. Characterizations

#### 3.1.1. PXRD

The poor water soluble and bioavailability of CUR provide the motivation for discovering novel solid forms to improve its the aqueous solubility. In our previous study, CUR-piperazine coamorphous phase, which with improved dissolution rate, was successfully screened [15]. Piperazine was chosen as coformer because it is commonly used

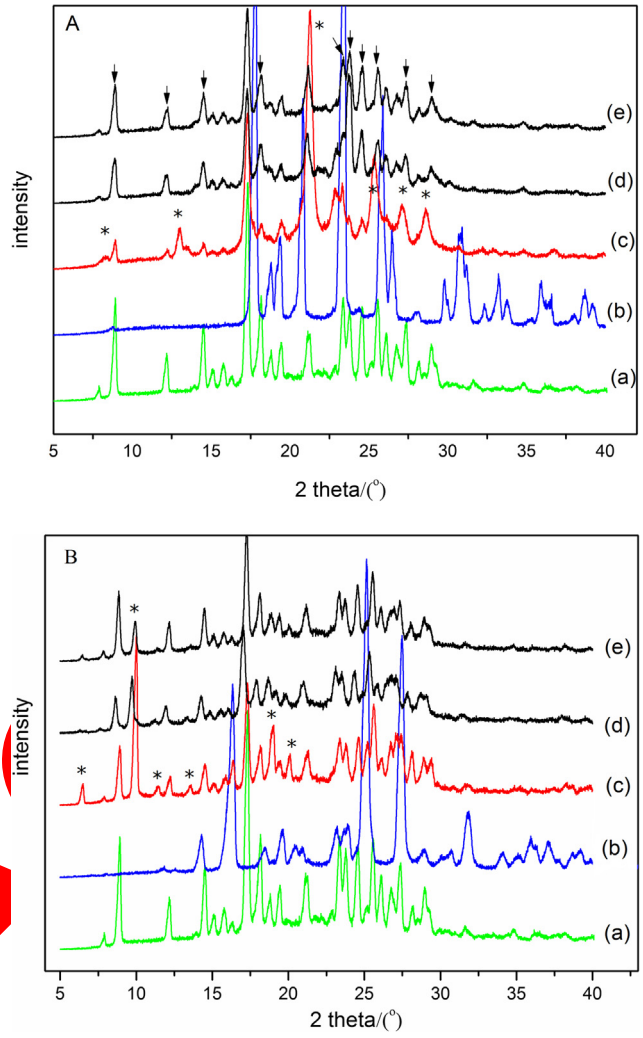


**Fig. 2.** PXRD patterns of the CUR-based cocrystals system (*: peaks for the new crystalloid complex; ↓: peaks for single CUR) A: (a) CUR (b) Isonicotinamide (c) CUR/isonicotinamide 1:2 (d) CUR/isonicotinamide 1:1 (e) CUR/isonicotinamide 2:1; B: (a) CUR (b) Gallic acid (c) CUR/gallic acid 1:2 (d) CUR/gallic acid 1:1 (e) CUR/gallic acid 2:1.

pharmaceutical intermediates and has piperazine ring with imino group (hydrogen donor). However, this piperazine-induced coamorphous phase showed extremely low $T_g$, which limited its pharmaceutical application. Generally, in the screening of cocrystal, the selection of coformers should be as broad as possible to achieve more solid states. Meanwhile, stand as candidate drugs, the coformers should be within the "generally recognized as safe (GRAS)" list so that the screened cocrystal is safe enough for human application. Thus, we choose herein isonicotinamide and gallic acid as coformers owing to their desirable hydrogen bonding donors and acceptors. Most importantly, isonicotinamide and gallic acid have intrinsic pharmacological activity, which has potential to produce drug-drug cocrystal [25].

The PXRD patterns of samples by varying the CUR/isonicotinamide in 2:1, 1:1 and 1:2 M ratios were shown in Fig. 2A. As seen in pattern of sample with the CUR/isonicotinamide in 1:2 M ratio (Fig. 2A-c), new peaks were observed at $2\theta$ = 8.3°, 13.0°, 27.1°, 28.5°, which were apparently different from CUR or isonicotinamide, suggesting appearance of new phase. Generally, along with the appearance of new peaks, disappearance of peaks corresponding to starting materials should be also observed if cocrystal is formed. As a result, peaks at 18.1°, 21.1°, 23.7°, 25.5°, 26.1°, 27.4°, and 28.9° belong to intact CUR and almost all peaks of isonicotinamide disappeared in PXRD pattern of

sample in 1:2 M ratio. However, when CUR was co-ground with isonicotinamide in the molar ratios of 2:1 and 1:1, almost all peaks indicative of CUR were observed and no obvious new peaks appeared (Fig. 2A-d, e). Suggestively, the combination prepared by the EtOH-assisted grinding method was cocrystal in nature when the ratio of CUR/isonicotinamide was 1:2. Notably, the PXRD pattern of as-prepared CUR-isonicotinamide cocrystal was different from that in patent WO 2015/052568A2 [10]. In the absence of single crystal XRD of the two cocrystals, it is difficult to give the difference on their structures. In patent WO 2015/052568A2, cocrystal was produced in ethyl acetate in refluxing condition at 80 °C, while, EtOH-assisted grinding method was used in our work. Solid states with different structures were produced using diverse screening method. For example, CUR-piperazine coamorphous phase was produced using EtOH-assisted grinding method in our previous work [15], while, CUR-piperazine cocrystals with CUR/piperazine in 2:1 and 1:1 M ratio were screened in refluxing condition at 45 °C in methanol and acetonitrile solvents, respectively, in patent WO 2015/052568A2. Not only the method but the solvent would have effect on the structure of the cocrystal, sometimes, solvent is introduced into the lattice of the cocrystal [26].

Likewise, PXRD pattern of CUR-gallic acid complexes with CUR/gallic acid in 1:2 M ratio exhibited obvious new characteristic reflections other than parent CUR and gallic acid at $2\theta$ = 6.5°, 9.9°, 11.4°, 13.6°, 18.9°, 20.1° (Fig. 2B-c), however, not all new peaks appeared in patterns of samples in 2:1 and 1:1 M ratios (Fig. 2B-d, e). It indicated that a new CUR-gallic acid cocrystal was produced in 1:2 M ratio.

### 3.1.2. SEM analysis

SEM can be used as a supplementary technique to characterize the formation of supramolecular new phases. The SEM images of CUR and its cocrystals were presented in Fig. 3. As can be seen, crystalline single CUR appears hexagonal block-shape (Fig. 3A), while the morphology of cocrystal 1 was a long non-hexagonal irregular rod (Fig. 3B). Crystalline single gallic acid shows fibrous microscopic morphology (Fig. 3C), however, it thoroughly loses the parent fibrous shape in cocrystal 2. SEM images of cocrystal 2 presents neither fibrous nor hexagonal short rods, but rather smaller particles shape (Fig. 3D). In conclusion, both changed microstructure and external morphology provided the evidence for the formation of cocrystal complexes between CUR and CCFs, correspondingly.

### 3.1.3. Thermal analysis

The thermal stabilities of CUR cocrystals 1 and 2 were examined by DSC. The DSC thermograms of CUR, CCFs and their cocrystals were shown in Fig. 4. CUR, isonicotinamide and cocrystal 1 showed melting point peaks at 178.4, 161.0, and 155 °C, respectively (Fig. 4A). Obviously, the melting point of cocrystal 1 was lower than those of CUR and isonicotinamide. However, the enthalpy of fusion of the cocrystal 1 (119.6 $J{\cdot}g^{-1}$) was higher than CUR (103.9 $J{\cdot}g^{-1}$) but lower than that of isonicotinamide (146.7 $J{\cdot}g^{-1}$), indicative of the formation of a different crystal lattice other than those of the two parent components upon cocrystallization. Likewise, the melting point of cocrystal 2 (174.8 °C) was lower than those of CUR and gallic acid (272.0 °C) (Fig. 4B), accompanied with the changing of enthalpy of fusion from CUR and gallic acid (366.4 $J{\cdot}g^{-1}$) to cocrystal 2 (116.0 $J{\cdot}g^{-1}$).

### 3.1.4. FT-IR spectroscopy

The formation of non-covalent forces such as hydrogen bonds between CUR and coformer in CUR supramolecular system can be analyzed by IR spectrum [15]. The overlaid IR spectra of cocrystal 1 system are presented in Fig. 5A. The stretching vibrations of phenolic O—H and C═O of the CUR and N—H in isonicotinamide located at 3505, 1626 and 3368 $cm^{-1}$, respectively. Briefly, the absorption peak at 3368 $cm^{-1}$ in isonicotinamide shifted to 3339 $cm^{-1}$ in cocrystal 1. The IR vibrations of the hydrogen bonding acceptor and donor generally shift to low wave numbers of 20–50 $cm^{-1}$ before and after hydrogen bond formation [27]. The shift of N—H group in isonictinamide is accordance with this law. The vibration peak of C═O in CUR showed no obvious change before and after cocrystal 1 formation. However, based on the movement of the vibration absorption of N—H in isonicotinamide, we can preliminarily deduce that the hydrogen bond in cocrystal 1 occurred between N—H group in isonicotinamide and certain hydrogen bond acceptor in CUR.

The IR spectra of cocrystal 2 system were shown in Fig. 5B. Gallic acid showed characteristic absorption peaks at 1669 $cm^{-1}$ and 3493 $cm^{-1}$ assigned to the carbonyl C═O and O—H stretching vibration, respectively (Fig. 5B-b), which showed no obvious shift in cocrystal 2. However, absorption peak of phenolic O—H stretching in CUR at 3505 $cm^{-1}$ disappeared or overlaid by O—H stretching vibration from gallic acid after the formation of cocrystal 2 (Fig. 5B-c). It maybe indicated that the hydrogen bonding in cocrystal 2 was formed between phenolic O—H in CUR and the hydrogen acceptor in gallic acid.

### 3.1.5. ssNMR and TD $^1H$ NMR

Only IR spectra are not enough to give the definite information of hydrogen bonds in cocrystals. $^{13}C$ ssNMR spectroscopy was employed to provide more information about differences in molecular conformations and bonding patterns. In the study of CUR-piperazine coamorphous [15], we noted significant changes in the chemical shifts for coamorphous phase. When API and CCF are bound by non-covalent weak forces, such as hydrogen bonds, the chemical shifts of the C atoms which take part in the formation of weak forces in the API and CCF molecules will change. The $^{13}C$ CP-MAS ssNMR spectra of single CUR, the CCFs and cocrystals are presented in Fig. 6. The corresponding $^{13}C$ chemical shifts were listed in Tables S2 and S3 (Supporting Information). As can be seen from Fig. 6A-a, the C9 and C11 in the CUR correspond to the carbonyl C atoms of ketone and enol (δ ~186.4, 182.0 ppm), indicating existence both ketone and enol C atoms in the molecular structure of single CUR. However, for cocrystal 1, only one sharp peak (δ ~183.8 ppm) appeared in the spectrum (Fig. 6A-a, c), provided information that the introduction of isonicotinamide stabilized the di-keto structure and the two C═O groups interacted with two isonicotinamide molecules in cocrystal 1 with the ratio of CUR/isonicotinamide 1:2. Moreover, owing to the conjugation effects of the double C═O groups, the chemical shifts for C8 and C12, C7 and C13, C4 and C14, C2 and C18 showed significant changes (Table S2). For isonicotinamide molecule, briefly, the $^{13}C$ chemical shift at 172.4 ppm assigned to carbonyl C adjacent N—H shifted to 170.9 ppm by virtue of bonding (Fig. 6A-b, c). In a conclusion, chemical shift of carbonyl C in CUR and isonicotinamide provided additional characterization of new solid phase cocrystal 1.

As for cocrystal 2, changes in ssNMR spectra showed some difference compare with cocrystal 1. The chemical shifts of C9 and C11 in cocrystal 2 did not merge into one peak, but the peak positions changed (δ ~186.4, 182.0 ppm shifted to 187.7, 183.3 ppm), then it may be inferred that both ketone and enol C atoms still coexisted in cocrystal 2. Obviously, the changes in the weak forces of C═O in cocrystal 2 were different from that of in cocrystal 1. Moreover, the chemical shifts of C1 and C17 assigned to phenolic O—H in CUR shifted from 158.2 to 159.5 ppm in cocrystal 2, suggesting the formation of weak interactions involving the phenolic O—H in CUR. However, the chemical shifts of the C atoms in gallic acid showed no obvious shift before and after cocrystallization (Table S3), for example, the upfield chemical shift of carbonyl C atom was only 0.2 ppm. According to the analysis of IR spectra, it is preliminarily confirmed that the hydrogen bonds was produced between phenolic O—H in CUR and the C═O group in gallic acid cocrystal 2. $^{13}C$ ssNMR spectra just gave the evidence that the phenolic O—H in CUR participated in hydrogen bonds as donor. The possible reason for nearly invariant chemical shift of C atoms in gallic acid before and after formation of cocrystal is existence of intrinsical hydrogen bond in gallic acid, that is, the C═O···H—O hydrogen bonds exist in homogeneous dimer in gallic acid owing to the contribution of

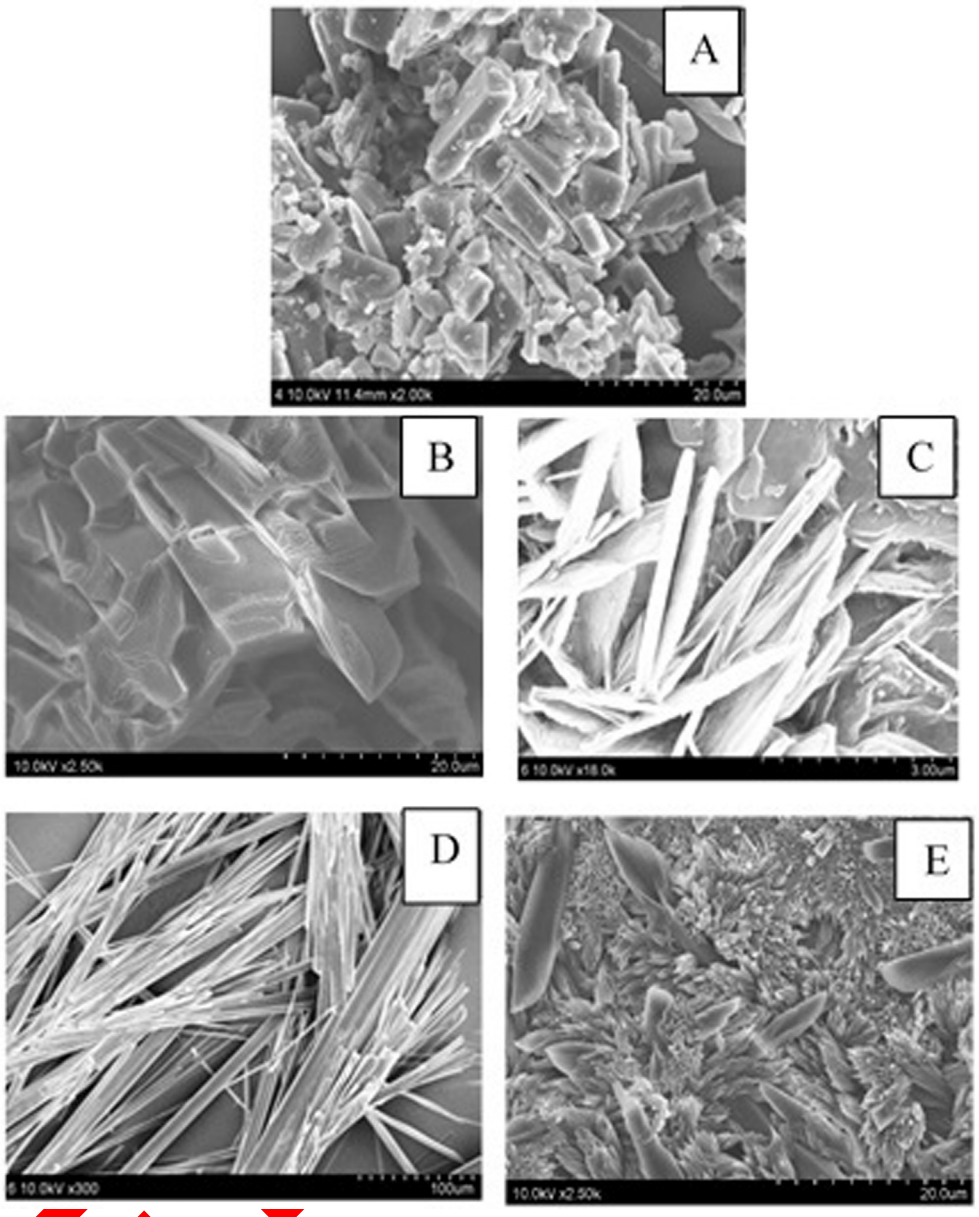


**Fig. 3.** Cryo-field emission SEM photographs of CUR and its cocrystals. (A) CUR (B) Isonicotinamide (C) Cocrystal 1 (D) Gallic acid (E) Cocrystal 2.

carboxyl groups [28]. When CUR was introduced into the lattice of gallic acid, the homomeric interactions was destroyed, then, the heteromeric system (cocrystal) between one CUR and two gallic acid molecules was formed through the same type C═O···H—O hydrogen bonds, which resulted in no obvious change in the chemical shift of C atoms in cocrystal 2.

The NMR relaxometry, i.e. $T_1$ and $T_2$ relaxation, is sensitive to local molecular motions, and has been widely used to characterize the molecular dynamics of various systems [29]. In order to discriminate the molecular dynamics difference of CUR before and after formation of cocrystals, the TD $^1$H NMR was used here to obtained the $T_1$ of different samples as shown in Fig. 7. As a comparison, the physical mixtures of CUR and CCFs were used. The $T_1$ values of CUR-isonicotinamide system showed difference with 1.71 s for CUR-isonicotinamide cocrystal, whereas those of pure CUR and its physical mixture with isonicotinamide were 1.61 and 1.47 s, respectively (Fig. 7A). In general, in the solid state, the lower the molecular mobility, the longer the $T_1$ relaxation time [30]. The longer $T_1$ relaxation time of CUR-isonicotinamide cocrystal (1.71 s) comparing with its physical mixture (1.47 s) at ambient temperature suggested a lower molecular mobility, which was due to the weak force between CUR and isonicotinamide in cocrystal. However, such longer $T_1$ in cocrystal did not occur in CUR-gallic acid system; $T_1$ values of cocrystal and physical mixture were almost the same (1.73 s for cocrystal and 1.72 s for physical mixture) at ambient temperature (Fig. 7B). The reason is that the gallic acid molecule has long $T_1$ relaxation time of 9.4 s (Figure not shown). Such long $T_1$ value of gallic acid even induced prolonged $T_1$ in physical mixture of CUR and gallic acid, which concealed decreasing of the molecular mobility coming from the weak force in cocrystal. The dynamics difference between cocrystal and physical mixture was not enough to give valid support on the interaction state in cocrystal for CUR-gallic acid system because that CCF molecule has too long $T_1$ relaxation time.

The reasonable configurations for the cocrystals 1 and 2 were simulated using the GAUSSIAN-03 program. The plausible models of the two heterogeneous trimers are shown in Fig. 8. The simulating reasonable configurations supported existence of above-mentioned hydrogen bonds deduced from IR and NMR spectra.

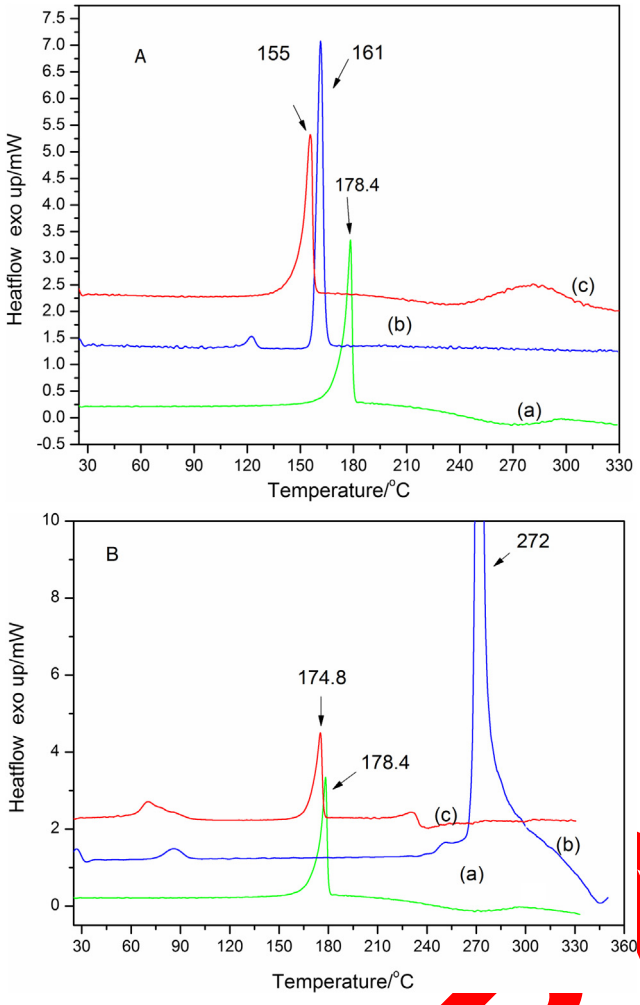


**Fig. 4.** DSC thermograms of the CUR, CCFs and its cocrystals. A: (a) CUR (b) Isonicotinamide (c) Cocrystal 1; B: (a) CUR (b) Gallic acid (c) Cocrystal 2.

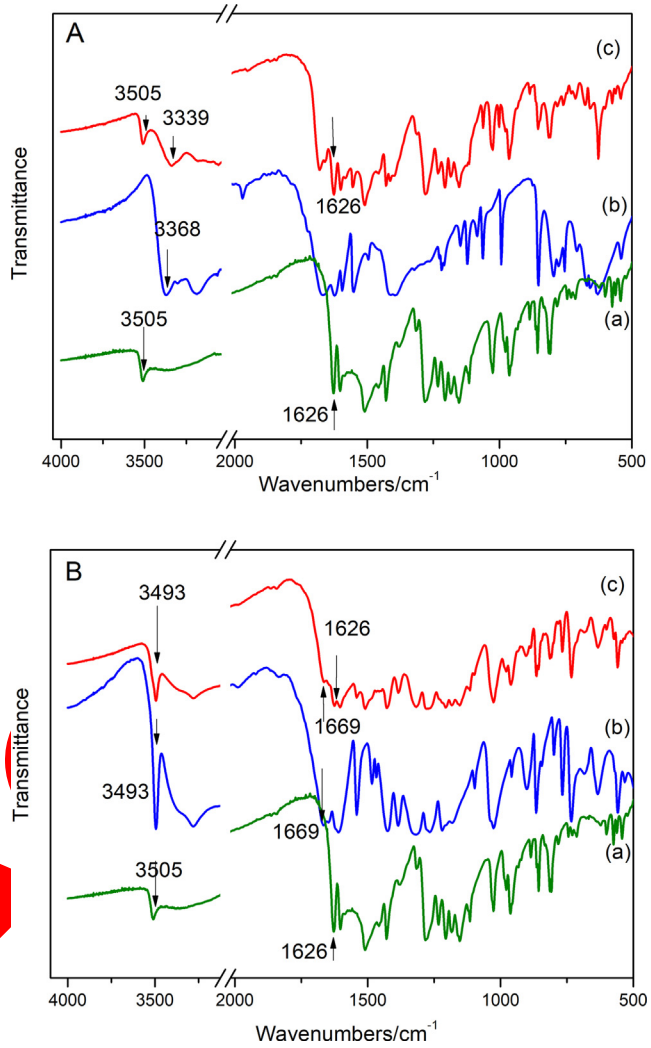


**Fig. 5.** IR spectra of the CUR, CCFs and its cocrystals. A: (a) CUR (b) Isonicotinamide (c) Cocrystal 1; B: (a) CUR (b) Gallic acid (c) Cocrystal 2.

### 3.2. Dissolution rate in vitro and pharmacokinetic in vivo

#### 3.2.1. Apparent solubility and powder dissolution rate

The solubility of single CUR is high under EtOH and acetone media but low in aqueous, acidic and neutral pH media [31]. The solubilities of CUR and its cocrystals in 0.1 mol·L$^{-1}$ HCl and 30% EtOH-water media were determined and presented in Table 1. It was found that crystalline CUR showed very low solubility in 0.1 mol·L$^{-1}$ HCl and 30% EtOH-water media. However, the solubilities of cocrystals were significantly improved compared with single CUR in 30% ethanol solution ($P < 0.05$), whereas the values showed no change in 0.1 mol·L$^{-1}$ HCl.

In order to show significant difference on solubility between CUR and its cocrystal, 0.1 mol·L$^{-1}$ HCl with 0.1% sodium dodecyl sulfate (SDS) (Fig. 9A) as well as 30% EtOH-$H_2O$ media (Fig. 9B) were used as dissolution media, in which they have higher dissolution rates. In those two media, the two cocrystals showed improvement on dissolution rate ($p < 0.05$). However, even with the help of SDS, the dissolution rate in 0.1 mol·L$^{-1}$ HCl was slower than that in EtOH-$H_2O$ media, which consisted with the result of solubility determination. In 30% EtOH-$H_2O$ media, the peak values were 58.69, 78.94, and 70.32% for single CUR, cocrystal 1 and 2, respectively, and the corresponding $t_{50}$ values were 103.6, 23.0 and 31.3 min. The dissolution rate of cocrystal 1 was 5-fold higher than that of single CUR ($p < 0.05$), suggesting a greater potential in solid form development for CUR because of its faster dissolution performance. Moreover, the inverse correlation between the melting point and solubility occurred in CUR and its cocrystals, that is, CUR, which has highest melting point (178.4 °C), showed lowest solubility and dissolution rate, whereas, for cocrystal 1, performed lowest melting point (155.0 °C) but highest solubility and dissolution rate.

#### 3.2.2. Pharmacokinetic parameters

Aside from improving the solubility and dissolution rate, the eventual goal of cocrystal screening is to improve the bioavailability of an API. The mean plasma concentration-time curves of CUR, cocrystal 1 and 2 after oral administration to rats are shown in Fig. 10, and the relevant pharmacokinetic parameters are listed in Table S4.

A "single-peak" was observed in both curves, thereby indicating that both CUR and its cocrystals followed the one compartment model. It is clear from the result that the pharmacokinetic parameters $C_{max}$, $T_{max}$, $AUC_{0-t}$ and $AUC_{0-\infty}$ of cocrystals were significantly improved ($P < 0.05$) by cocrystallization (Table S4). For example, in the case of cocrystal 1, $C_{max}$ increased about 30-fold (2.06 ± 0.28 ng·mL$^{-1}$ for single CUR and 64.87 ± 26.79 ng·mL$^{-1}$ for cocrystal 1), $T_{max}$ shortened about 6-fold (1.59 ± 1.00 h for single CUR and 0.27 ± 0.12 h for cocrystal 1), $AUC_{0-t}$ raised about 7-fold than that of single CUR (6.96 ± 1.56 ng·h·mL$^{-1}$ for single CUR and 46.90 ± 7.71 ng·h·mL$^{-1}$ for cocrystal 1).

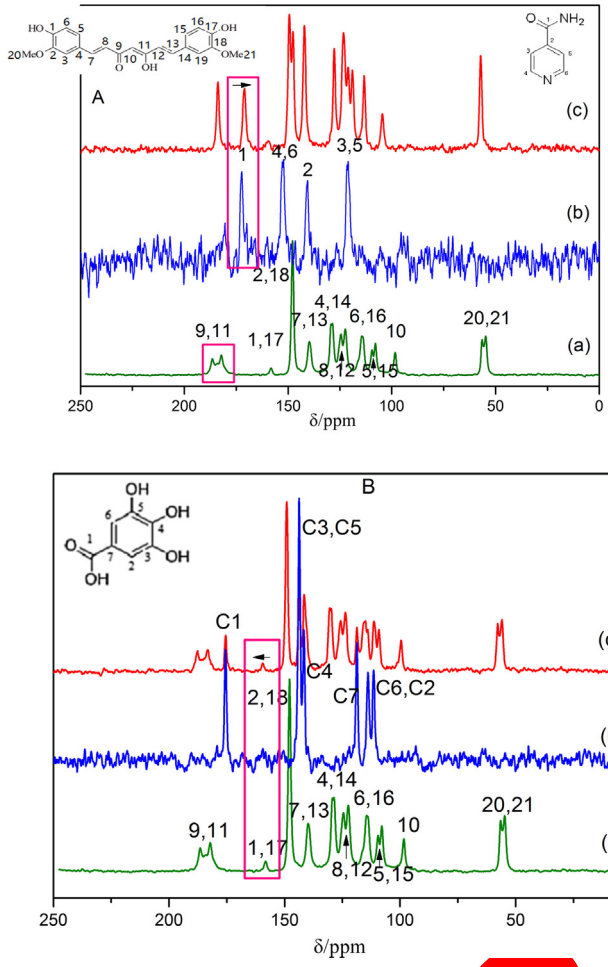


**Fig. 6.** Overlay of $^{13}C$ ssNMR spectra of the CUR, CCFs and cocrystals. A: (a) CUR (b) Isonicotinamide (c) Cocrystal 1; B: (a) CUR (b) Gallic acid (c) Cocrystal 2.

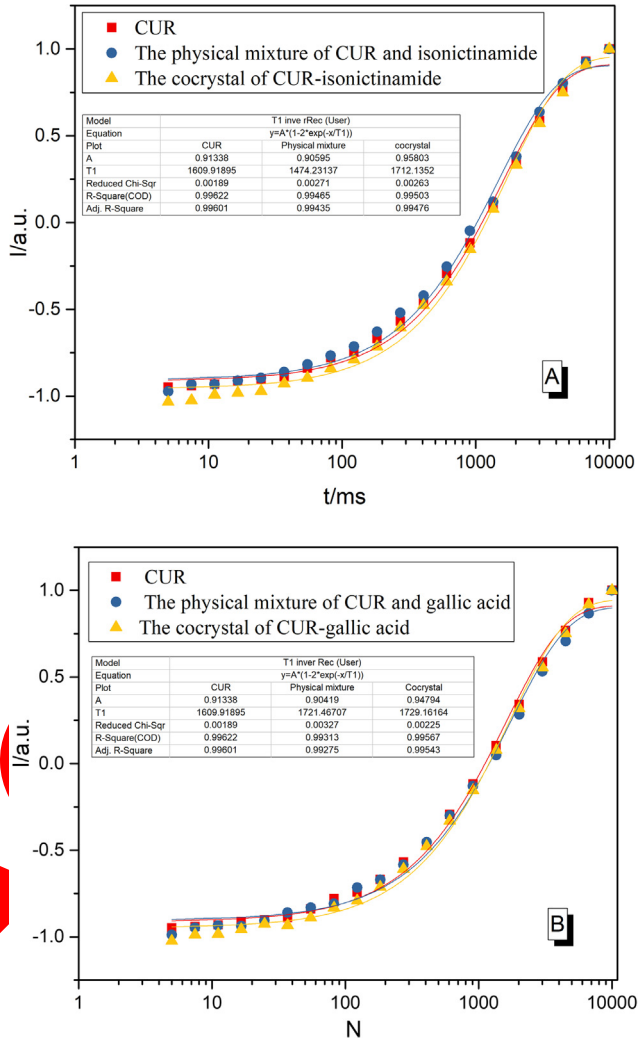


**Fig. 7.** The $T_1$ relaxation time of CUR-isonicotinamide system (A) and CUR-gallic acid system (B).

### 3.3. Fluorescence spectroscopic studies on the interaction of CUR-based cocrystals with BSA

#### 3.3.1. Fluorescence quenching mechanism of BSA

As is well known, the binding manner of API-protein is related with absorption, distribution, metabolism, elimination and even pharmacological profile of drugs [32]. Firstly, we focused on the effects of the type of hydrogen bonds occurred in cocrystal on the binding between cocrystal and BSA. Fluorescence quenching of BSA or HSA in the presence of API as quencher, which can provide adequate informations including binding mechanism, binding-specific parameters, and structural changes of the protein, is commonly applied to characterize the interaction of API molecules with proteins. The mechanism of fluorescence quenching can be divided into two types: dynamic and static quenching [33], which follow the Stern-Volmer Eq. (1) and Lineweaver-Burk double reciprocal Eq. (2), respectively.

$$\frac{F_0}{F} = 1 + K_{sv}[Q] = 1 + K_q \tau 0 [Q] \quad (1)$$

$$\log[(F_0 - F)/F] = \log K_b + n \log[Q] \quad (2)$$

where $F$ and $F_0$ are the fluorescence intensity in the presence and absence of quencher, respectively. $[Q]$ is the concentration of CUR. $K_{sv}$ is the Stern-Volmer dynamic quenching constant, a direct measure of the quenching efficiency [34], and $K_q$ is the quenching rate constant of biomolecule. $K_b$ is apparent static binding constant and $n$ is the average number of binding sites per protein molecule. The temperature-dependent behavior of $K_{sv}$ can be used to judge quenching mechanisms.

Used Stern-Volmer Eq. (1), the fluorescence quenching data at different temperatures (i.e., 298, 310 and 315 K) were adopted to analyze the quenching mechanism in CUR and its crystals on BSA. The $K_{sv}$ values obtained from Stern-Volmer plots of $F_0/F$ against CUR concentration were listed in Table S5. It can be seen, the $K_{sv}$ values decreased with temperature increasing, and the values of $K_q$ were greater than the maximum diffusion impact quenching constant of $2 \times 10^{10} \cdot s^{-1} \cdot mol^{-1}$ [35]. Moreover, the $K_{sv}$ and $K_q$ values of the samples were negatively correlated with the temperature, which indicated that the quenching mechanism of CUR and its cocrystals were all static quenching. However, the calculated values of $K_{sv}$ for single CUR were different from those of cocrystals, for example, quite higher than that of cocrystal 2. It was suggested that the hydrogen bonding occurred in cocrystals induced the change on the interaction between CUR and BSA.

#### 3.3.2. Binding constant and thermodynamic parameters

The Lineweaver-Burk double reciprocal Eq. (2) was used to calculate the binding constants and the number of binding sites of API with BSA [36]. By using $\log[(F_0 - F)/F]$ as the ordinate and $\log[Q]$ as the abscissa, the slope $n$ and intercept $\lg K_b$ of the straight line are obtained by linear fitting (Fig. 11). The values of the binding constants of CUR and its cocrystal were listed in Table 2.

Based on the $K_b$ values, enthalpy change values ($\Delta H^\theta$), entropy value ($\Delta S^\theta$) and the free energy change ($\Delta G^\theta$) of binding reaction of API and

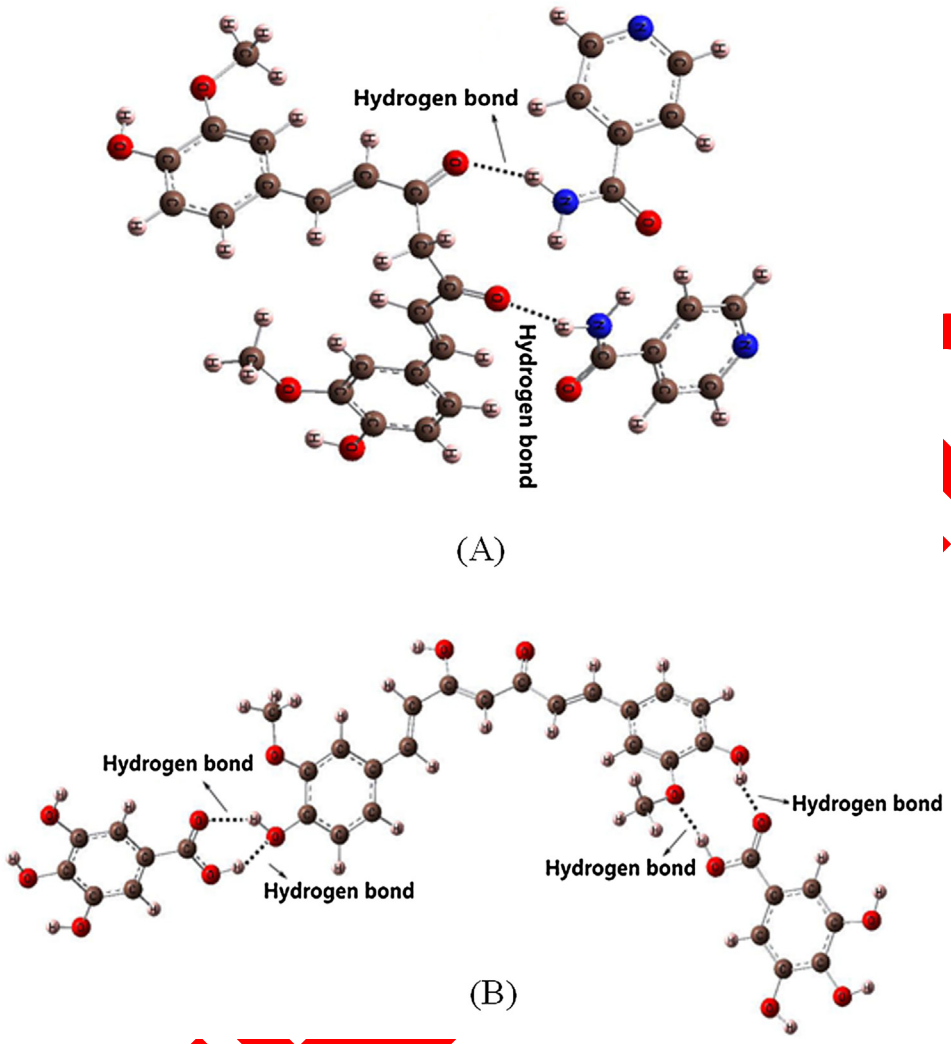


**Fig. 8.** Simulated plausible models of the interactions (hydrogen bonds are marked using dashed lined) between CUR and CCFs in trimer for cocrystal 1 (A) and 2 (B). Modeling was conducted using a GAUSSIAN-03 program package at the DFT B3lyp/6-31**level.

**Table 1**
Solubility of CUR and its complexes in various media at 310 K (n = 3, $x \pm s$).

| Samples | Solubility ($\mu g \cdot mL^{-1}$) | |
|---|---|---|
| | 0.1 $mol \cdot L^{-1}$ HCl | 30% ethanol |
| CUR | 10.10 ± 3.31 | 17.9 ± 2.81 |
| Cocrystal 1 | 11.58 ± 3.71 | 77.1 ± 3.11 |
| Cocrystal 2 | 11.39 ± 3.83 | 72.6 ± 3.63 |

BSA can be calculated by Van't Hoff Eq. (3) and Gibbs-Helmholtz Eq. (4) (Table 2) [37]:

$$\ln K_b = -\Delta H^\theta / RT + \Delta S^\theta / R \quad (3)$$

$$\Delta G^\theta = \Delta H^\theta - T\Delta S^\theta \quad (4)$$

As can be seen in Table 2, $K_b$ values showed an inverse correlation with the temperatures for CUR and co crystal 1, confirming the static quenching on BSA. However, the $K_b$ values of the cocrystal 2 increased with the increase of temperature, suggesting a dynamic quenching process on BSA. Combined with the result of $K_{sv}$ above, we speculated that the interaction between cocrystal 2 and BSA was the process of static quenching accompanied by dynamic quenching.

Generally, there are four types of weak interactions between API (quencher) and BSA biological macromolecules: hydrogen bonding, van der Waals, hydrophobic and electrostatic interactions [38]. We can use the magnitude and sign of $\Delta H^\theta$ and $\Delta S^\theta$ to judge the types of force(s) in API-BSA interaction, that is, negative $\Delta H^\theta$ and $\Delta S^\theta$ values suggest both hydrogen bonds and/or van der Waals forces, while positive $\Delta H^\theta$ and $\Delta S^\theta$ values indicate the presence of hydrophobic interactions. Obviously, hydrogen bonds and/or van der Waals forces played a major role in the binding of CUR and cocrystal 1 to BSA due to the negative $\Delta H^\theta$ and $\Delta S^\theta$ (Table 2). Also, negative $\Delta H^\theta$ and $\Delta S^\theta$ indicated an exothermic and enthalpy-driven binding reaction between CUR and BSA. However, the positive $\Delta H^\theta$ and $\Delta S^\theta$ suggested the presence of hydrophobic interaction in the binding of cocrystal 2 to BSA.

The differences on $K_b$ and type of weak interactions of CUR-BSA and cocrystal-BSA indicated that the introduction of CCF changed the binding manner of CUR to BSA. As evidenced by IR and ssNMR above, different hydrogen bond occurred in cocrystal 1 and 2, namely C═O···H—N hydrogen bonds in cocrystal 1 and the O—H···O═C hydrogen bond in cocrystal 2. Those mentioned above hydrogen bonds occurred in solid state cocrystal supramolecules. When API-CCF cocrystal dissolves into API and CCF molecules in solution, the crystalline structure is broken and some intermolecular weak forces lost. Speculation was reasonable that, although intermolecular weak forces between API and CCFs in solid state cocrystal were broken in solution, some new, similar and more flexible intermolecular weak forces were rebuilt (*vide infra*). For cocrystal 1, in solution, if the C═O groups in CUR was involved in formation of hydrogen bonds just same as in solid state, then, the

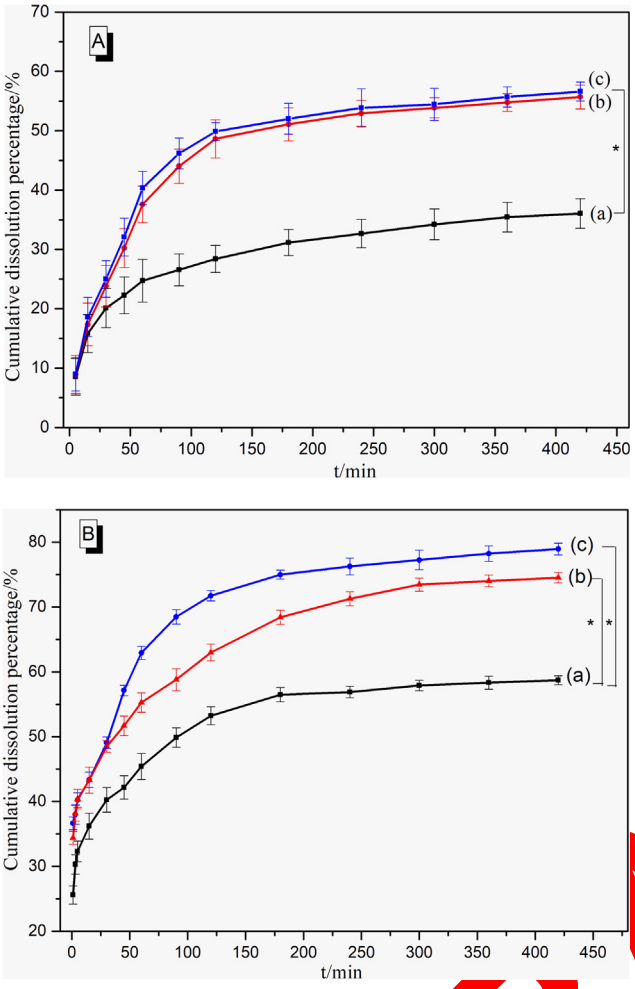


**Fig. 9.** Powder dissolution curves in 0.1 mol·L$^{-1}$ HCl with 0.1% SDS (A) and 30% EtOH-water medium (B). CUR (b) Cocrystal 2 (c) Cocrystal 1 (310 ± 0.5 K, n = 3, $x$ ± s) (*$P$ < 0.05).

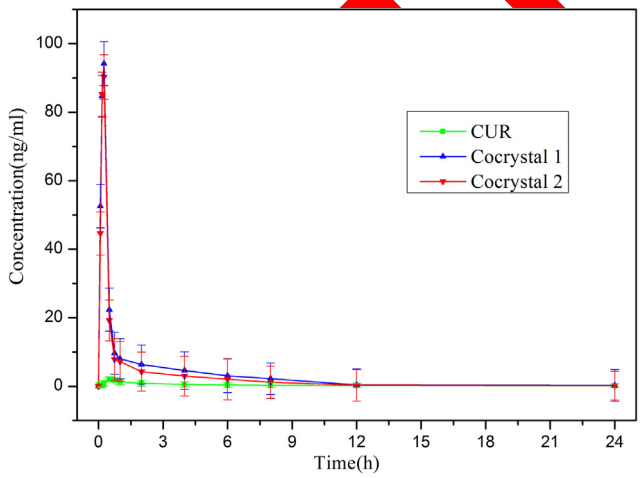


**Fig. 10.** Mean plasma concentration-time curves of CUR and its cocrystals in rats after oral administration (n = 6, $\bar{\chi}$ ± s).

terminal phenolic O—H or methyl C—H groups tended to form hydrogen bond during the binding between biomacromolecule BSA. However, with regard to cocrystal 2, if phenolic O—H groups in CUR participate in formation of weak forces in solution, it was difficult for C═O or methyl C—H groups to bind with hydrogen bond acceptor and donor in BSA owing to the steric effect. As a result, hydrophobic interaction, other than hydrogen bond in CUR-BSA binding reaction, occurred with the introduction of gallic acid. We also found the same result in CUR-piperazine coamorphous phase [15]. When CUR connected with piperazine through hydrogen bond occurred between C═O on CUR and H-N in piperazine, the binding profiles of CUR-BSA was different from that of CUR-piperazine-coamorphous-BSA. More evidences showed that the weak interactions between API and coformer in cocrystal/coamorphous supramolecular complex affected its weak interaction with other protein molecules.

### 3.3.3. Conformational investigations

Synchronous fluorescence spectroscopy [39] was used to analyze the effect of CUR on the conformation of proteins after formation of supramolecular system. The fluorescence of protein mainly comes from tryptophan and tyrosine residues, and the change of protein conformation was analyzed by the change of Δλ [40]. The characteristic fluorescence spectra of tryptophan and tyrosine residues correspond to Δλ = 60 and 15 nm, respectively.

The synchronous fluorescence spectra of CUR and its cocrystals were provided in Fig. S1. The fluorescence intensity of tryptophan and tyrosine residues decreased with the increasing of sample concentration. The position of the emission peak of tyrosine residues did not change both for cocrystal 1 and 2, indicating that CUR and its cocrystal mainly affected the microenvironment near the tryptophan residues in BSA. However, the emission peaks of tryptophan (Δλ = 60 nm) in the presence of CUR and cocrystal 1 showed a certain degree of blue shift, while cocrystal 2 appeared red shift. The movement of the emission peak of tryptophan residues was related to the weak force between API and CCF. It was observed that different kinds of hydrogen bonding in cocrystal led to the different shifts (blue shift for cocrystal 1 and red shift for cocrystal 2) of emission peak of the tryptophan residues, reflecting the effect on the conformation of BSA.

### 3.4. Cytotoxicity test results

Plentiful evidences support CUR's use in cancer prevention owing to its anticarcinogenic and antiproliferative properties though various action mechanisms, including inhibiting proliferation of colon cancer cell lines (HT-29) by accumulating cells in G2-M phase [41], apoptosis in NIH3T3 and leukemic cell line HL-60 [42] and through the generation of reactive oxygen species [43]. In this work, we selected three kinds of cancer cells, including human colon cancer cells (HT-29), lung cancer cells (A549) and hepatoma cells (Hepg), to perform the MTT assays for CUR and its cocrystals. The cell inhibitions at different CUR concentration after 24 h were presented in Figs. S2 and S3 and corresponding $IC_{50}$ values were listed in Table 3.

The resulting growth curves show that CUR possesses a dose-dependent inhibitory effect on three kinds of cancer cells (Figs. S2 and S3). While, it was found the inhibitory rate of CUR to HT-29 was best. For cocrystal 1, the cytotoxicity to HT-29, A549 and Hepg cells showed no statistical change compared with those of single CUR, confirming that the cell cytotoxicity of the cocrystal 1 did not affect by the introduction of isonicotinamide coformer. However, for cocrystal 2, the results were somewhat complicated. Gallic acid, which is coformer in cocrystal 2, is not a simple CCF, but has pharmacological activities, such as anticancer, antiradical, anti-inflammatory and antioxidant [44]. So, we also performed MTT assay on gallic acid. MTT results indicated that gallic acid showed cytotoxicity to HT-29, A549 and Hepg cells and the best inhibitory rate was found to A549 cell ($IC_{50}$ ~ 25.7 ± 2.9 μg·mL$^{-1}$), indicating differential sensitivity to different cell type (Figs. S2 and S3). However, for cocrystal 2, the cytotoxicity to HT-29 and Hepg cells was lower than that of single CUR at higher CUR concentration ($P$ < 0.05), while inhibitory rate to A549 cell showed no obvious change. These observations suggested that negative synergism action occurred in cocrystal 2. With introduction of

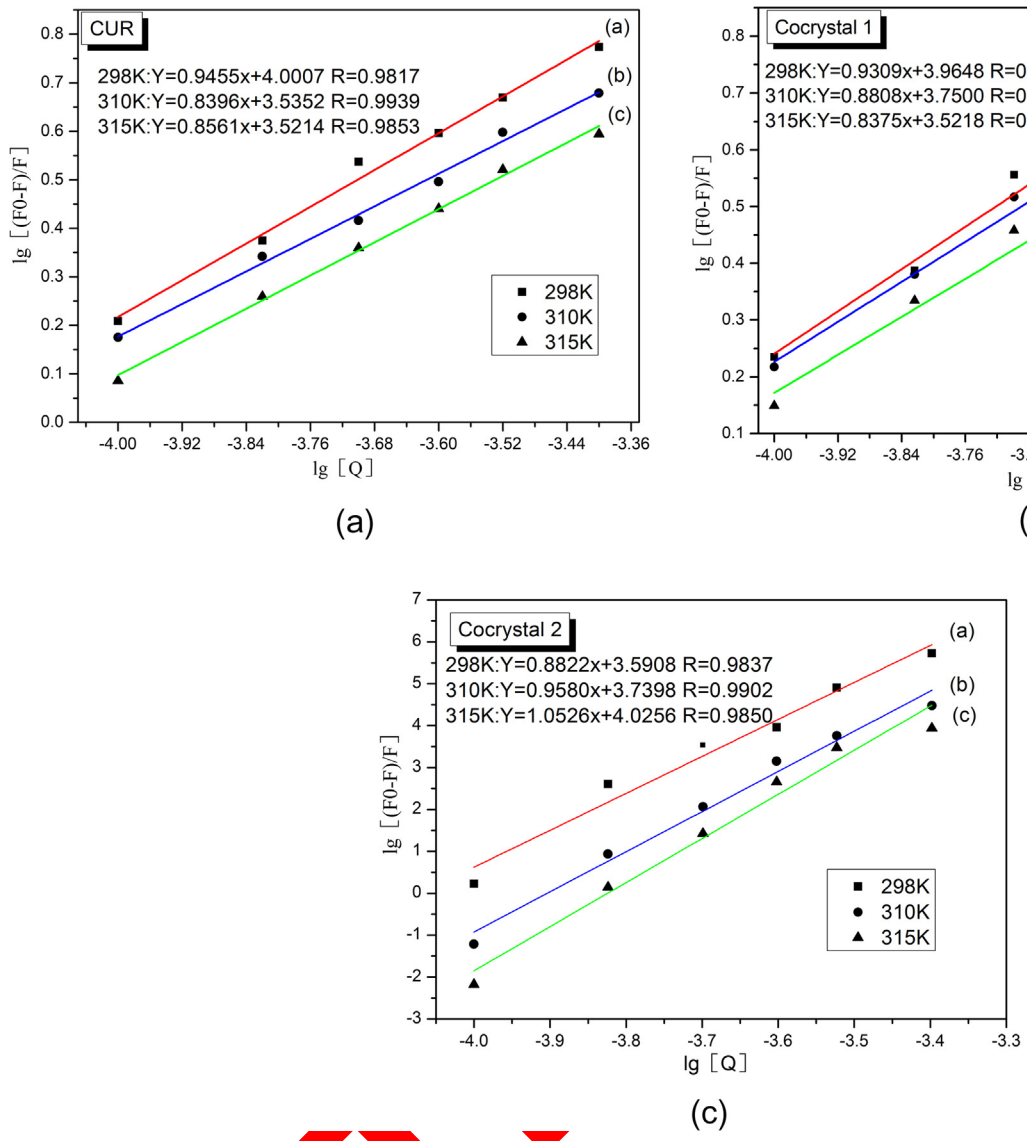


**Fig. 11.** Modified Stern-Volmer plots of CUR and its cocrystals interaction with BSA at (a) 298 K (b) 310 K (c) 315 K. $C_{BSA} = 5 \times 10^{-6}$ mol·L$^{-1}$.

CCF gallic acid, the inhibitory rate of cocrystal 2 to cancer cells was not improved, instead, dramatically decreased compared with that of single CUR.

The different cell inhibitory profiles of the cocrystal 1 and 2 give us speculation again of that some new, similar and more flexible intermolecular weak forces were rebuilt between API and CCF molecules in solution after bulk cocrystal dissolves. For that, we performed solution NMR; the $^{13}$C NMR spectra of cocrystal 1 and 2 systems in DMSO solvent were provided in supporting information (Fig. S4). When API-CCF cocrystal dissolves into API and CCF molecules in solution, the crystalline structure is broken and some intermolecular weak forces lost, the solution NMR shows different information compared with ssNMR. The solution NMR spectra of cocrystals show all the peaks of pure CUR and the chemical shifts show no obvious shift compared with pure CUR, suggesting that the pure CUR is released from the cocrystal structure in solution. However, chemical shifts of small molecule CCF,

**Table 2**
Binding constant $K_b$ and thermodynamic parameters of the CUR and its cocrystal-BSA system at different temperatures.

| Samples | T/K | $K_b$/($10^3$ L·mol$^{-1}$) | $\Delta H^\theta$/(kJ·mol$^{-1}$) | $\Delta S^\theta$/(J·mol$^{-1}$·K$^1$) | $\Delta G^\theta$/(kJ·mol$^{-1}$) |
|---|---|---|---|---|---|
| CUR | 298 | 10.0 | | | −22.7 |
| | 310 | 3.4 | −54.2 | −105.7 | −21.5 |
| | 315 | 3.3 | | | −20.9 |
| Cocrystal 1 | 298 | 9.2 | | | −22.7 |
| | 310 | 5.6 | −43.9 | −71.0 | −21.9 |
| | 315 | 3.3 | | | −21.5 |
| Cocrystal 2 | 298 | 3.9 | | | −20.3 |
| | 310 | 5.5 | 41.3 | 206.6 | −22.8 |
| | 315 | 10.6 | | | −23.8 |

**Table 3**
The $IC_{50}$ values of CUR, cocrystal 1, 2 and gallic acid against HT-29, Hepg and A549 cells ($n = 3$, $\bar{\chi} \pm S$).

| Cells | $IC_{50}$($\mu g \cdot mL^{-1}$) | | | |
|---|---|---|---|---|
| | CUR | Cocrystal 1 | Gallic acid | Cocrystal 2 |
| HT-29 | 30.6 ± 3.4 | 25.3 ± 2.9 | 42.1 ± 2.4* | 36.1 ± 2.4 |
| Hepg | 34.9 ± 3.1 | 34.3 ± 2.6 | 40.2 ± 2.8 | 38.5 ± 2.5 |
| A549 | 33.7 ± 2.7 | 32.8 ± 2.3 | 25.7 ± 2.9* | 29.2 ± 2.3 |

* $P < 0.05$ vs single CUR.

isonicotinamide and gallic acid, showed changes, even some peaks disappear in cocrystal solution. For example, the chemical shifts at 167.94 and 166.96 ppm assigned to carbonyl C in isonicotinamide and gallic acid, respectively, shift to 169.08 and 166.79 ppm in their respective cocrystal solution. Besides, new peaks appear in cocrystal solution. Obvious new peaks at 145.68, 138.43 and 108.98 ppm appeared in the NMR of CUR-isonicotinamide cocrystal; and 150.91 in CUR-gallic acid cocrystal. The new peaks maybe from splitting of origin peaks or improving strength of origin extremely weak peaks owing to some rebuilt intermolecular forces between API and CCF molecules in solution.

Intermolecular weak forces would induce the change of electrostatic potentials of API [15], as a result, led to the change of action on cell. Although the types of weak forces were not clear, different shift of peak in isonicotinamide and gallic acid and different new peaks appearance suggested various intermolecular weak forces, which produce different cell cytotoxicity.

Up to date, it has not a clear argument which group in CUR molecule play a role in the inhibitory effect in the various biological models and particularly on the HT-29, A549 and Hepg cells. In CUR molecule, phenolic hydroxyl groups, phenolic methoxyl groups and the diketone moiety are the potential active parts responsible for inhibitory effect. Delage et al. reported that the diketone moiety appeared to be the part of the CUR molecule involved in the antiproliferative effect on MCF-7 cell proliferation [45]. MTT assays showed that the cell cytotoxicity of the cocrystal 1 showed no obvious change by the introduction of isonicotinamide, while, for cocrystal 2, the cytotoxicity to HT-29 and Hepg cells was lower than that of single CUR. It inferred that various intermolecular weak forces in two cocrystals solution gave rise to different effect on the active group in CUR. We need more CUR-based cocrystal samples to investigate the relationship between the weak interactions occurred in cocrystal and the cell cytotoxicity on the various type cells, which promotes the future research on CUR-based cocrystal screening.

## 4. Conclusion

Most reports on cocrystal concern about the improvement on solubility, dissolution rate and even bioavailability of API. CUR-based cocrystal 1 and 2 showed significant higher solubility, dissolution rate and even bioavailability in vivo than that of single CUR ($P < 0.05$). Screening of CUR-based cocrystal supramolecular complexes has the potential to be a novel strategy to improve the pharmacokinetics as parameters of $C_{max}$, $T_{max}$ and bioavailability of CUR. Most importantly, in present study, this is the first time to demonstrate the effects induced by the different types of weak forces in cocrystal on binding with BSA and cell cytotoxicity. CUR-based cocrystal 1 and 2 provided us suitable models to investigate the relationship between the weak interactions in cocrystal and the biological profiles of the APIs. The binding mechanism and binding forces of API-CCF supramolecular complex with BSA and cell inhibitory rates vary with the kinds of weak forces between API and CCF. Based on our observations, we would venture to speculate that the cocrystal maybe retain some of the interactions in the solid state when it dissolves in solution. Although, we need more evidences to achieve the “general rule” on the relationship between the kinds of weak force in cocrystal and the binding mechanism with protein molecules/biological activity, this study highlights the importance of performing appropriate investigations on cocrystal as a new chemical entity but not single API.

## Declaration of Competing Interest

The authors have declared no conflict of interest.

## Acknowledgment

The financial support for this work by the Education Department of Hebei Province of China through innovative hundred talents support program (SLRC2017047) is greatly acknowledged. Thanks are also due to National Natural Science Funds of China (Grant No. 81202504) and the Natural Science Foundation of Hebei Province (Grant No. H2017206214). The TD NMR characterization in this work by National Synchrotron Radiation Laboratory, Anhui Provincial Engineering Laboratory of Advanced Functional Polymer Film, CAS Key Laboratory of Soft Matter Chemistry, University of Science and Technology of China, Hefei, China, is also acknowledged.

## Appendix A. Supplementary material

Supplementary data to this article can be found online at https://doi.org/10.1016/j.ejpb.2019.05.005.

## References

[1] A.B. Kunnumakkara, D. Bordoloi, G. Padmavathi, J. Monisha, N.K. Roy, Curcumin, the golden nutraceutical: multitargeting for multiple chronic diseases, Br. J. Pharmacol. 174 (2017) 1325–1348.
[2] J.A. Seo, B. Kim, D.N. Dhanasekaran, B.K. Tsang, Y.S. Song, Curcumin induces apoptosis by inhibiting sarco/endoplasmic reticulum Ca(2+) ATPase activity in ovarian cancer cells, Cancer Lett. 371 (2016) 30–37.
[3] D. Hao, J. Wang, W. Lu, X. Tang, J. Chen, Curcumin inhibited HGF-induced EMT and angiogenesis through regulating c-Met dependent PI3K/Akt/mTOR signaling pathways in lung cancer, Mol. Ther. Oncolytics 3 (2016) 16018–16022.
[4] M. Merlos, E. Portillo-Salido, A. Brenchat, B. Aubel, J. Buxens, A. Fisas, X. Codony, L. Romero, D. Zamanillo, J.M. Vela, Administration of a co-crystal of tramadol and celecoxib in a 1:1 molecular ratio produces synergistic antinociceptive effects in a postoperative pain model in rats, Eur. J. Pharmacol. 833 (2018) 370–378.
[5] C. Almansa, R. Mercè, N. Tesson, J. Farran, J. Tomàs, Co-crystal of tramadol hydrochloride-celecoxib (ctc): a novel API-API co-crystal for the treatment of pain, Cryst. Growth Des. 17 (2017) 1884–1892.
[6] K. Löbmann, H. Grohganz, R. Laitinen, S. Clare, T. Rades, Amino acids as coamorphous stabilizers for poorly water soluble drugs-part 1: preparation, stability and dissolution enhancement, Eur. J. Pharm. Biopharm. 85 (2013) 873–881.
[7] D. Walsh, D.R. Serrano, Z.A. Worku, B.A. Norris, A.M. Healy, Production of co-crystals in an excipient matrix by spray drying, Int. J. Pharm. 536 (2018) 467–477.
[8] M. Alsubaie, M. Aljohani, A. Erxleben, P. McArdle, Co-crystal forms of the BCS class IV drug sulfamethoxazole, Cryst. Growth Des. 7 (2018) 3902–3912.
[9] C.D. Lao, M.T. Ruffin, D. Normolle, D.D. Heath, S.I. Murray, Dose escalation of a curcuminoid formulation, BMC Complem. Altern. Med. 6 (2006) 10–13.
[10] S. Chava, S.R.A. Gogantla, V.K. Muppidi, Solid forms of curcumin and derivatives therefor, WO 2015/052568A2.
[11] I. Sathisaran, S.V. Dalvi, Crystal engineering of curcumin with salicylic acid and hydroxyquinol as coformers, Cryst. Growth Des. 17 (2017) 3974–3988.
[12] S.F. Chow, L.M. Shi, W.W. Ng, K.H.Y. Leung, K. Nagapudi, C.C. Sun, A.H.L. Chow, Kinetic entrapment of a hidden curcumin cocrystal with phloroglucinol, Cryst. Growth Des. 14 (2014) 5079–5089.
[13] K. Suresh, M.K.C. Mannava, A. Nangia, A novel curcumin-artemisinin coamorphous solid: physical properties and pharmacokinetic profile, RSC Adv. 4 (2014) 58357–58361.
[14] J.M. Skieneh, I. Sathisaran, S.V. Dalvi, S. Rohani, Co-amorphous form of curcumin-folic acid dihydrate with increased dissolution rate, Cryst. Growth Des. 17 (2017) 6273–6280.
[15] W.Z. Pang, J. Lv, S. Du, J.J. Wang, J. Wang, Y.L. Zeng, Preparation of curcumin-piperazine coamorphous phase and fluorescence spectroscopic and density functional theory simulation studies on the interaction with bovine serum albumin, Mol. Pharm. 14 (2017) 3013–3024.
[16] H.G. Brittain, Cocrystal systems of pharmaceutical interest, Cryst. Growth Des. 12 (2012) (2010) 1046–1054.
[17] H.G. Brittain, Cocrystal systems of pharmaceutical interest, Cryst. Growth Des. 12 (2012) (2011) 5823–5832.
[18] V. Ferretti, A. Dalpiaz, V. Bertolasi, L. Ferraro, S. Beggiato, F. Spizzo, E. Spisni, B.A. Pavan, Indomethacin co-crystals and their parent mixtures: does the intestinal barrier recognize them differently? Mol. Pharm. 12 (2015) 1501–1511.

[19] A.B. Kunnumakkara, P. Anand, B.B. Aggarwal, Curcumin inhibits proliferation, invasion, angiogenesis and metastasis of different cancers through interaction with multiple cell signaling proteins, Cancer Lett. 269 (2008) 199–225.
[20] W.D. Lu, Y. Qin, C. Yang, L. Li, Effect of curcumin on human colon cancer multidrug resistance in vitro and in vivo, Clinics 18 (2013) 694–701.
[21] B.Y. Du, L.P. Jiang, Q. Xia, L. Zhong, Synergistic inhibitory effects of curcumin and 5-Fluorouracil on the growth of the human colon cancer cell line HT-29, Chemotherapy 52 (2006) 23–28.
[22] C. Syng-Ai, A.L. Kumari, A. Khar, Effect of curcumin on normal and tumor cells: Role of glutathione and bcl-2, Mol. Cancer Ther. 3 (2004) 1101–1108.
[23] H. Wu, Q. Liu, T. Cai, Y.D. Chen, Z.F. Wang, Induction of microRNA-146a is involved in curcum in-mediated enhancement of temozolomide cytotoxicity against human glioblastoma, Mol. Med. Rep. 12 (2015) 5461–5470.
[24] M.J. Frisch, G.W. Trucks, H.B. Schlegel, et al., GAUSSIAN 03 (Revision D.01), Gaussian, Inc., Wallingford, CT, 2004.
[25] B. Khodayar, M.H. Farzaei, A.H. Abdolghaffari, R. Bahramsoltani, M. Baeiri, F. SabbaghZiarani, The protective effect of the gallic acid against TNBS-induced ulcerative colitis in rats: role of inflammatory parameters, J. Iranian Med. Council 1 (1) (2018) 34–42.
[26] W. Guo, S. Du, Y.L. Lin, B. Lu, C.Q. Yang, J. Wang, Y.L. Zeng, Structural and computational insights into the enhanced solubility of dipfluzine by complexation: salt and salt-cocrystal, New J. Chem. 42 (2018) 15068–15078.
[27] Y.L. Lin, H. Yang, C.Q. Yang, J. Wang, Preparation, characterization, and evaluation of dipfluzine-benzoic acid co-crystals with improved physicochemical properties, Pharm. Res. 31 (2014) 566–578.
[28] D.E. Braun, R.M. Bhardwaj, A.J. Florence, D.A. Tocher, S.L. Price, Complex polymorphic system of gallic acid-five monohydrates, three anhydrates, and over 20 solvates, Cryst. Growth Des. 13 (2013) 19–23.
[29] O. Kotaro, H. Daijiro, K. Shungo, K. Atsushi, H. Yoshihiro, O. Yoshinori, $^{1}$H NMR relaxation study to evaluate the crystalline state of active pharmaceutical ingredients containing solid dosage forms using time domain NMR, J. Pharm. Sci. 108 (2019) 451–456.
[30] N. Bloembergen, E.M. Purcell, R.V. Pound, Relaxation effects in nuclear magnetic resonance absorption, Phys Rev. 73 (7) (1948) 679–712.
[31] S. Qureshi, A.H. Shah, A.M. Ageel, Toxicity studies on alpinia galangal and curcuma longa, Planta Med. 58 (1992) 124–127.
[32] D. Pangeni, C. Kapil, M.A. Jairajpuri, P. Sen, Inter-domain helix h10DOMI-h1DOMII is important in the molecular interaction of bovine serum albumin with curcumin: spectroscopic and computational analysis, Eur. Biophys. J. 44 (2015) 139–148.
[33] G.F. Shen, T.T. Liu, Q. Wang, Spectroscopic and molecular docking studies of binding interaction of gefitinib, lapatinib and sunitinib with bovine serum albumin (BSA), J. Photochem. Photobiol. B 153 (2015) 380–390.
[34] C. Dufour, O. Dangles, Flavonoid-serum albumin complexation: determination of binding constants and binding sites by fluorescence spectroscopy, Biochim. Biophys. Acta 1721 (2005) 164–173.
[35] M.A. Rub, J.M. Khan, A.M. Asiri, R.H. Khan, Study on the interaction between amphiphilic drug and bovine serum albumin: a thermodynamic and spectroscopic description, J. Lumin. 155 (155) (2014) 39–46.
[36] D.J. Li, Y. Wang, J.J. Chen, B. Ji, Characterization of the interaction between farrerol and bovine serum albumin by fluorescence and circular dichroism, Spectrochim., Acta A 79 (2011) 680–686.
[37] M. Jiang, M.X. Xie, G.D. Zheng, Y. Liu, X.Y. Li, Spectroscopic studies on the interaction of cinnamic acid and its hydroxyl derivatives with human serum albumin, J. Mol. Struct. 692 (2004) 71–80.
[38] A. Sulkowska, J. Rownieka, B. Bojko, W. Sułkowski, Interaetion of anticancer drugs with human and bovine serum albumin, J. Mol. Struct. 651 (2003) 133–140.
[39] N. Cacita, S. Nikolaou, Studying the interaction between trinuclear ruthenium complexes and human serum albumin by means of fluorescence quenching, J. Lumin. 169 (2016) 115–120.
[40] K.N. Baglole, P.G. Boland, B.D. Wagner, Fluorescence enhancement of curcumin upon inclusion into parent and modified cyclodextrins, J. Photochem. Photobiol. A 173 (2005) 230–237.
[41] R. Hanif, L. Qiao, S.J. Shiff, B. Rigas, Curcumin a natural plant phenolic food additive, inhibits cell proliferation and induces cell cycle changes in colon adenocarcinoma cell lines by a prostaglandin independent pathway, J. Lab. Clin. Med. 130 (1997) 576–584.
[42] M.L. Kuo, T.S. Huang, J.K. Lin, Curcumin, an antioxidant and antitumor promoter, induces apoptosis in human leukemia cells, Biochim. Biophys. Acta 1317 (1996) 95–100.
[43] A. Khar, A.M. Ali, B.V.V. Pardhasaradhi, C. Varalakshmi, R. Anjum, A.L. Kumari, Induction of stress response renders human tumor cell lines resistant to curcumin-mediated apoptosis: role of reactive oxygen intermediates, Cell Stress Chaperon. 6 (2001) 368–376.
[44] F. Reza, N. Laura, Antioxidant potency of gallic acid, methyl gallate and their combinations in sunflower oil triacylglycerols at high temperature, Food Chem. 244 (2018) 29–35.
[45] A. Simona, D.P. Allaisb, J.L. Durouxc, J.P. Baslyd, F.S. Durand, C. Delage, Inhibitory effect of curcuminoids on MCF-7 cell proliferation and structure-activity relationships, Cancer Lett. 129 (1998) 111–116.